Simulated CLAS12 Neutron Detection Efficiency in the Forward Time-of-Flight System

G.P. Gilfoyle[1], M.Ungaro[2], J. Carbonneau[1], M. Moog[1], and C. Musalo[1]

[1] *University of Richmond, Richmond, VA*
[2] *University of Connecticut, Storrs, CT*

October 1, 2011

Abstract

We have simulated the production of quasi-elastically (QE) scattered electrons and neutrons in CLAS12 with the physics-based, CLAS12 simulation package *gemc*. The electron events were reconstructed with *Socrat*. We have studied the properties of the deposited energy and efficiency of the CLAS12 FTOF system to establish a baseline for the future measurement of the neutron magnetic form factor in Experiment E12-07-104. We have simulated the extraction of the neutron detection efficiency using QE neutrons and found an efficiency of 16% for panels P1A and P1B combined together and a value of 8% for panel P2B. A comparison of the simulated efficiency using only panels P1A and P2B (that are being reused from CLAS6) with the measured values from the E5 run (using the $^1\mathrm{H}(e, e'\pi^+)n$ reaction) shows good agreement.

1 Introduction

In this CLAS-NOTE we present the results of a study of the efficiency for detecting quasielastic neutrons in the CLAS12 forward time-of-flight (FTOF) system. We are preparing for experiment E12-07-104 entitled 'Measurement of the Neutron Magnetic Form Factor at High Q^2 Using the Ratio Method on Deuterium' where the ratio of quasielastic (QE) $e-n$ to $e-p$ scattering is measured and the neutron magnetic form factor G_M^n is extracted [1]. The QE $e-n$ scattering will be measured separately with the CLAS12 forward TOF system (FTOF) and the forward electromagnetic calorimeter (EC). We focus here on the performance of the FTOF. The neutron detection efficiency (NDE) must be accurately determined to meet the experimental goals of systematic uncertainties of 3% or less. We will also compare the simulated results found here with those measurements of the NDE performed for an earlier CLAS6 measurement of G_M^n during the E5 run. This comparison will be particularly relevant because some of the CLAS12 FTOF scintillators will be the same as the ones used in the E5 measurement. Experiment E12-07-104 was originally approved by PAC32 and reviewed by PAC35 to allocate beam time. Thirty days of running were awarded by PAC35 along with an A^- rating.

The format of this paper is the following. (1) The motivation for the experiment will be presented and (2) along with a description of the ratio method. (3) The results from a physics-based simulation (Geant4 Monte Carlo *gemc*) of the scintillator response to the passage of electrons and neutrons will be presented [2]. (4) The inputs and results will be shown from the *gemc* simulation of elastic $e-n$ scattering and reconstruction with the Root-based code Socrat [2, 3]. (5) Last, we will present the post-reconstruction analysis used to extract the neutron detection efficiency in the FTOF.

2 The CLAS12 G_M^n Experiment (E12-07-104)

In JLab Experiment E12-07-104 we intend to dramatically extend the reach of our understanding of a fundamental feature of the neutron: its magnetic form factor G_M^n. The elastic electromagnetic form factors(EEFFs) describe the distribution of charge and magnetization inside the nucleon at low Q^2 and probe the quark structure at higher Q^2. This experiment is part of a broad program at JLab to measure the EEFFs, map the internal landscape of the nucleon, and test non-perturbative Quantum Chromodynamics (QCD) and QCD-inspired models of the nucleon (see NSAC Long-Range Plan [4]). The measurement will cover the range $Q^2 = 3.5 - 13.5$ GeV^2 with systematic uncertainties less than 3%. Statistical uncertainties will be about 3% in the highest Q^2 bin in this range and significantly less at lower Q^2. The anticipated range and statistical uncertainties of the experiment are shown in Figure 1. The reduced magnetic form factor $G_M^n/(\mu_n G_D)$ is plotted versus Q^2 where μ_n is the neutron magnetic moment and $G_D = 1/(1 + Q^2/\Lambda^2)^2$ is the dipole form factor with $\Lambda^2 = 0.71$ GeV^2. We used the recent parameterization of the world's data on G_M^n in Ref [13] to predict the reduced form factor. Also shown are selected world's data for G_M^n including the recent CLAS6 results (blue, open circles)[5]. The proposed CLAS12 experiment (black, closed squares) will nearly triple the upper limit of the previous CLAS6 measurement and provide precise data well past any existing measurement.

3 The Ratio Method

To measure G_M^n we will use the ratio of quasielastic $e-n$ to quasielastic $e-p$ scattering on deuterium which has been used by us in CLAS6 [5] and others [9, 17, 18, 19, 20] to measure G_M^n (see Figure 1). The ratio method is less vulnerable to systematic uncertainties than previous methods and we will have consistency checks between different detector components of CLAS12 (the FTOF and the CLAS12 electromagnetic calorimeter (EC)) and an overlap with our previous CLAS6 measurements. A liquid-hydrogen/liquid-deuterium, dual target will be used to make *in situ* measurements of the neutron and proton detection efficiencies. We take advantage of the large acceptance of CLAS12 and veto events with additional particles (beyond $e-n$ and $e-p$ coincidences) to reduce the inelastic background. We expect to limit the systematic uncertainties to 3% or less [21]. This experiment can be done with the base equipment for CLAS12 and was approved by PAC32.

The method is based on the ratio of $e-n$ to $e-p$ scattering

$$R = \frac{\frac{d\sigma}{d\Omega}(^2\mathrm{H}(e,e'n)_{QE})}{\frac{d\sigma}{d\Omega}(^2\mathrm{H}(e,e'p)_{QE})} = a(Q^2)\frac{\sigma^n_{mott}(G_E^{n\,2}+\frac{\tau_n}{\varepsilon_n}G_M^{n\,2})\left(\frac{1}{1+\tau_n}\right)}{\frac{d\sigma}{d\Omega}(^1\mathrm{H}(e,e')p)} \quad (1)$$

for quasielastic (QE) kinematics. The right-hand side is written in terms of the free nucleon form factors and where $\tau = Q^2/4M^2$ and $\epsilon = 1/[1+2(1+\tau)\tan^2(\theta/2)]$. Deviations from this 'free ratio' assumption are parameterized by the factor $a(Q^2)$ which can be calculated from deuteron models and is close to unity at large Q^2. The results of other measurements of the

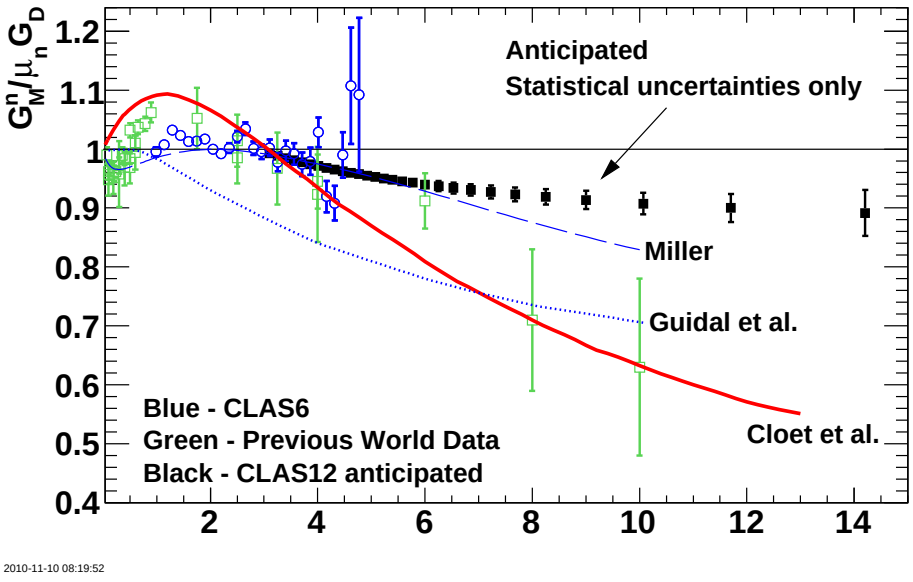

Figure 1: Selected data [5, 6, 7, 8, 9, 10, 11, 12] and anticipated results for G_M^n (black, filled squares) in units of $\mu_n G_D$ as a function of Q^2. The anticipated CLAS12 results follow a fit to the world data on G_M^n that includes the recent CLAS6 G_M^n results [13]. The blue, open circles are the CLAS6 results [5]. The curves are from Miller (blue, dashed,[14]), Guidal *et al.* (blue, dotted,[15]), and Cloët *at al.* (red,[16]).

proton cross section and the neutron electric form factor are used to extract G_M^n. The ratio R is insensitive to the luminosity, electron acceptance, electron reconstruction efficiency, trigger efficiency, the deuteron wave function used in $a(Q^2)$, and radiative corrections [5, 22].

An essential aspect of the neutron measurement in the FTOF and EC systems is measuring the neutron detection efficiency. In the experiment we will use the $^1\mathrm{H}(e, e'\pi^+ n)$ reaction as a source of tagged neutrons. Electrons and π^+'s will be detected in CLAS12 and missing mass used to select candidate neutrons that are expected to strike the active area of CLAS12. These particles are labeled 'found' neutrons. We predict the position of the neutron in CLAS12 and search for it in the FTOF hits. If a hit is detected near the expected position, we classify these particles as 'reconstructed' neutrons. The ratio of reconstructed to found events gives us the detection efficiency. This will be done in CLAS12 with a unique, dual target. Co-linear, liquid hydrogen and deuterium cells will provide production and calibration events simultaneously and under the same conditions (*in situ*). This reduces our vulnerability to variations in detector gains, beam properties, *etc.* The same method was used in the CLAS6 measurement during the E5 run period. The results for the NDE measurement at two different beam energies is shown in Figure 2.

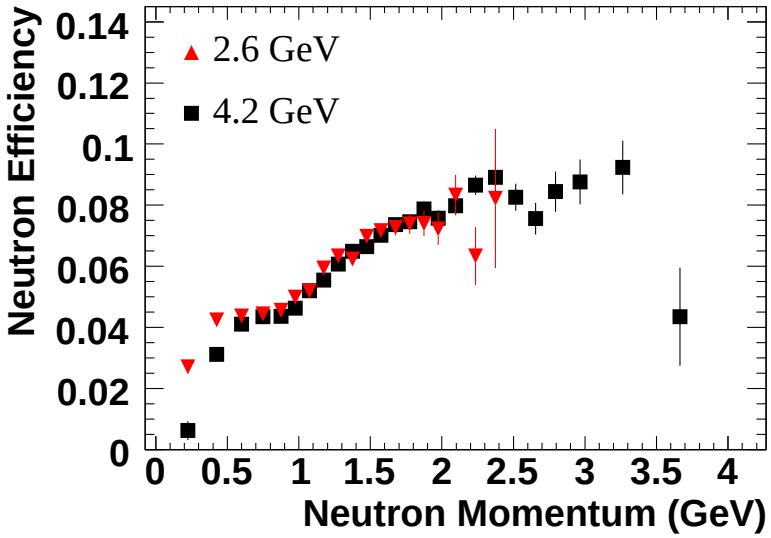

Figure 2: Neutron detection efficiency measured with the $^1\mathrm{H}e, e'\pi^+)n$ reaction for the CLAS6 G_M^n measurement.

For this study we do not yet have an appropriate simulation of the $^1\mathrm{H}(e, e'\pi^+)n$ reaction so we will start with a simulation of elastic scattering from a simulated neutron target as a first step to understanding the neutron detection efficiency. The method we will use is analogous to the one proposed for E12-07-104 and used in Ref [5]. Scattered electrons are simulated in CLAS12 and the electron information is used to predict the position of the neutron assuming that elastic scattering has occurred. If the predicted position of the neutron is within the active area of the FTOF we call this a found neutron. We then search the simulation results for a FTOF hit near the found neutron. If an FTOF hit is located

within an angular cone around the predicted position of the found neutron, then we have a reconstructed neutron. The NDE is the ratio of reconstructed to found neutrons.

4 Simulation of FTOF Scintillator Response to Electrons

The passage of electrons and neutrons through the scintillator material of the FTOF was simulated with *gemc*. The *gemc* code is a physics-based simulation using the Geant4 package from CERN [23]. It is an object-oriented, C^{++}-based code that reads detector information from an external, mysql database. Hits in detector components are built by a factory method at run time, and the output banks are dynamic. Qt4 is used for a graphical user interface [24].

The geometry of the FTOF is shown in Fig. 3 including the three FTOF panels in each sector labeled P1A, P1B, P2B. Most of the CLAS12 components have been removed to

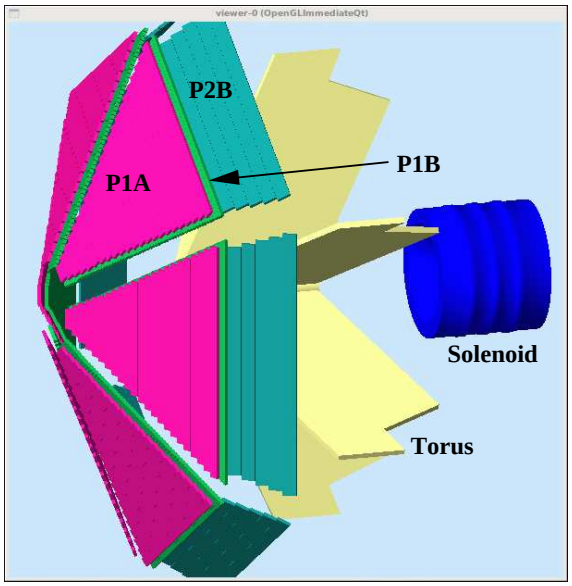

Figure 3: Geometry of the FTOF system.

make the FTOF system more visible. The CLAS12 torus and solenoid are shown to orient the reader. The layer labeled P1A (pink strips in Figure 3) consists of 23 strips that are each 15.0 cm wide and 5.08 cm thick. These are the same strips used in the current CLAS6 detector. The layer labeled P1B (bright green strips in Figure 3) just in front of the P1A panel in each sector consist of 58 strips that are each 6.0 cm wide and 6.0 cm thick. These scintillators will be new in CLAS12. The last FTOF panel in each sector is labeled P2B in Figure 3 and has scintillators that are 22 cm wide and 5.08 cm thick. These scintillators are also being reused from CLAS6. See the CLAS Technical Design Report for more details [25].

To study the FTOF response we simulated the interactions of electrons in the scintillators under special conditions. The *gemc* code was run for electrons at momenta that covered

the range expected for quasielastic events in that panel. Each electron was given a direction with a polar angle $\theta_e = 25°$ so it struck one of the strips perpendicular to the plane of the panel. Choosing this direction makes interpreting the results simpler because the sample of events is uniform (except for the different electron momenta) and there are no edge effects (all of the electrons strike the FTOF far from the FTOF edges). The other CLAS12 components between the target and the FTOF panel were removed in the simulation so those components would not alter the properties of the electrons striking the panel. The CLAS12 magnetic field was also turned off. This feature insures the electrons strike the face of the FTOF at a perpendicular angle. We analyzed the results using the just the hit information generated by *gemc* so we did not use the track reconstruction code *Socrat* [3] in this portion of the study. The *gemc* command is

```
gemc -gcard=p1a.gcard
```

where the contents of the input file `p1a.gcard` are described in Appendix A. The energy deposited for electrons in the P1A scintillator panel is shown in Figures 4-5 for electron momenta of 9.25 GeV/c and 3.5 GeV/c respectively. These momenta are at the upper and lower limits of the QE momentum range we expect to observe in the P1A scintillator. The left-hand panel of Fig. 4 shows the distribution of energy deposited in the scintillator

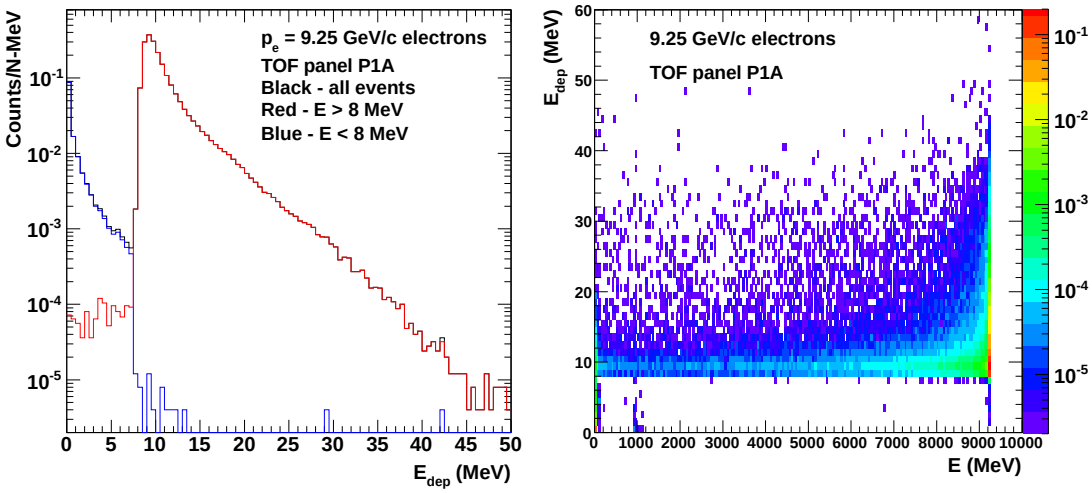

Figure 4: Energy deposited and particle energy in the FTOF scintillators for electrons of momentum $p_e = 9.25$ GeV for FTOF panel P1A. The vertical axis in the left-hand panel is the number of events from the Monte Carlo, *gemc* calculation divided by the bin size and the number of thrown events. The histogram in the right-hand panel is the number of events divided by the number of thrown events.

E_{dep} for all particles that leave any energy in the scintillator (black curve largely obscured by the other histograms). Electrons of momentum 9.25 GeV were simulated incident at one point near the center of the scintillator, and normal to the surface (to simplify the interpretation of the hit information). The spectra in Fig. 4 are for all particles, but nearly

all (98%) are electrons. The peak created by minimum-ionizing particles (MIPs) is visible at $E_{dep} \approx 9$ MeV. This peak is at the expected position since MIPs deposit about 2 MeV of energy per cm of scintillator material and panel P1A is 5 cm thick. There is also a significant number of events at energies below the MIP peak.

To understand the low-E_{dep} features below the MIPs, consider the right-hand panel of Fig. 4 which shows a two-dimensional histogram of E_{dep} versus E where E is the energy (known in simulation) of the particle as it enters the volume (the P1A scintillator panel here). The threshold at $E_{dep} \approx 8$ MeV is the low-E_{dep} edge of the MIP peak. Electrons passing through the scintillator are not expected to deposit energy less than this amount. There are narrow peaks at $E = 9.25$ GeV in the right-hand panel of Fig. 4 (corresponding to the incident electron energy) and at $E = 0$ MeV. The long, E tail below $E = 9.25$ GeV is due to primary electrons that have emitted a bremsstrahlung photon before reaching the P1A scintillator. At $E = 9.25$ GeV and $E_{dep} < 8$ MeV in the right-hand panel of Fig. 4 there is a low-E_{dep} tail below the energy of a minimum-ionizing particle. These events are due to full-energy electrons that enter the scintillator and emit a bremsstrahlung photon that carries away nearly all of the incident electron energy. The remaining, now low-energy, electrons will stop in the scintillator and deposit less than the MIP energy all the way down to zero. Another explanation for this high-E, low-E_{dep} tail is from backscattered electrons, but the cross section for bremsstrahlung is orders of magnitude greater than the backscatter one. This low-E_{dep}, high-E feature can be seen in the red histogram in the left-hand panel of Fig. 4 where the E_{dep} spectrum is extracted for events with $E > 8$ MeV; the minimum energy deposited for MIPs and the threshold visible in the right-hand panel. The red histogram almost completely overlaps the MIP peak and has the low-E_{dep} tail.

The blue histogram in the left-hand panel is for events with $E < 8$ MeV and corresponds to the peak near $E = 0$ MeV in the right-hand panel. These are low-E, secondary electrons produced when the primary electron passed through the scintillator. The thickness of the P1A scintillator (5 cm) corresponds to the range of electrons with energies of about 10 MeV so electrons with energies up to 10 MeV will stop in the scintillator (unless they are produced near the back surface of the panel so they can escape). Once the energy of the secondary electrons exceeds 10 MeV they will pass through the scintillator and deposit the MIP energy (unless they have a momentum that carries them along the long-axis of the scintillator paddle through a larger amount of the material). In the $E_{dep} - E$ distribution there is also a hint of protons that deposited energy in the scintillator at $E \approx 1$ GeV. These protons were produced by reactions in the scintillator.

We now consider the effect of lower incident momentum electrons on the FTOF response. Fig. 5 shows the results from the analysis of the same study illustrated in Fig. 4, but at a lower primary electron momentum corresponding to the momentum of quasielastic electrons near the large-angle edge of the FTOF panel P1A. The command used to generate the event file with *gemc* was the same used above with only the incident electron momentum changed. The left-hand panel of Fig. 5 shows the same E_{dep} distribution except now the incident electron momentum is 3.5 GeV. The overall shape of the distribution and its breakdown into components above and below the MIP threshold are nearly identical. The right-hand panel in Fig. 5 shows E_{dep} versus E distribution as in Fig. 4, but with the reduced incident electron momentum. The only difference is the reduced E range due to the lower incident momentum. For the range of electron momenta we have studied here the response of the

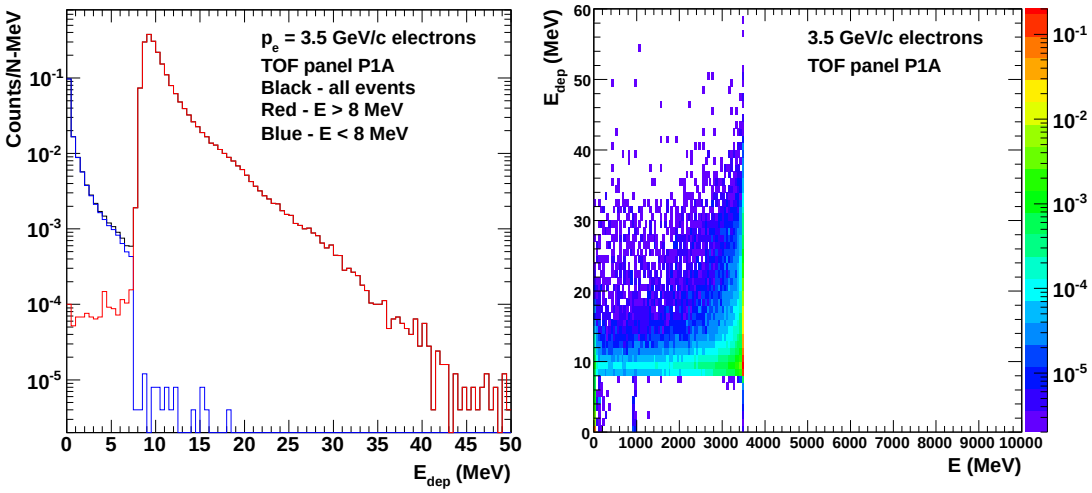

Figure 5: Energy deposited and particle energy in the FTOF scintillators for electrons of momentum $p_e = 3.5$ GeV for FTOF panel P1A. The vertical axis in the left-hand panel is the number of events from the Monte Carlo, *gemc* calculation divided by the bin size and the number of thrown events. The histogram in the right-hand panel is the number of events divided by the number of thrown events.

FTOF system to electrons is largely independent of the incident neutron momentum.

The response of the FTOF panel P1B is shown in Figs 6-7. These panels are mounted upstream of panel P1A (see Fig. 3), cover about the same angular range, and are thicker (6 cm versus 5 cm). As in the previous study, simulated, incident electrons at two momenta (3.5 GeV/c and 9.25 GeV/c) struck the center of the panel normal to the surface. Comparing Figs. 4 and 6 (9.25 GeV/c) the distributions are very similar. The only difference is the E_{dep} threshold for the minimum ionizing particles is higher in panel P1B than in panel P1A (9 MeV versus 8 MeV) because P1B is thicker. The same features can be seen comparing Figs. 5 and 7 (3.5 GeV/c).

The response of the FTOF panel P2B is shown in Fig. 8. This panel is mounted at larger angles relative to panel P1A (see Fig. 3), covers the angular range $\theta = 35^\circ - 45^\circ$, and has the same thickness as the P1A panels (5 cm). The scintillators will be reused from CLAS6. Simulated, incident electrons at momentum 2.5 GeV/c struck the center of the panel normal to the surface. We only used a single momentum here since the angular range and, hence, the momentum range for quasielastic electrons is narrow. Comparing Fig. 8 with the other panels shows that the minimum ionizing peak is much the same as the one for panel P1A which has the same thickness of scintillator. The shape of the E_{dep} spectrum changes little with incident electron beam energy as seen in comparing the left-hand panels in Figs. 4-8. In the two-dimensional plots of E_{dep} versus E, they all have similar features; the only difference is the position of the peak from the incident electrons.

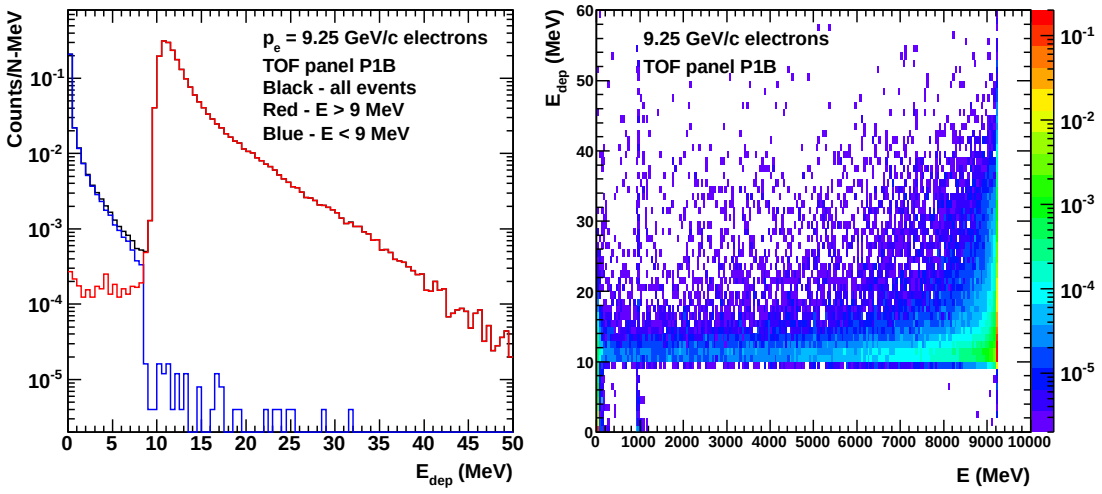

Figure 6: Energy deposited and particle energy in the FTOF scintillators for electrons of momentum $E = 9.25$ GeV/c for FTOF panel P1B. The vertical axis in the left-hand panel is the number of events from the Monte Carlo, *gemc* calculation divided by the bin size and the number of thrown events. The histogram in the right-hand panel is the number of events divided by the number of thrown events.

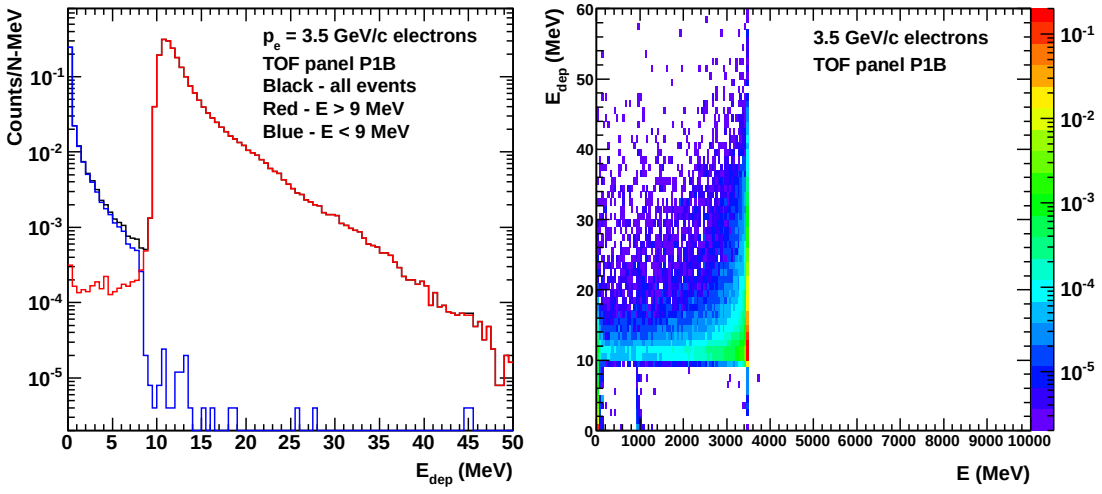

Figure 7: Energy deposited and particle energy in the FTOF scintillators for electrons of momentum $E = 3.5$ GeV/c for FTOF panel P1B. The vertical axis in the left-hand panel is the number of events from the Monte Carlo, *gemc* calculation divided by the bin size and the number of thrown events. The histogram in the right-hand panel is the number of events divided by the number of thrown events.

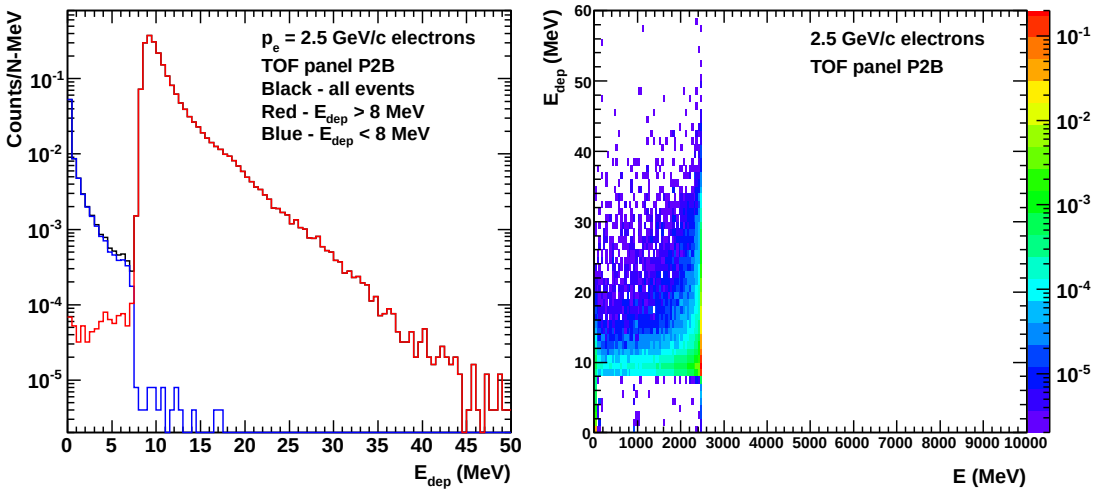

Figure 8: Energy deposited and particle energy in the FTOF scintillators for electrons of momentum $E = 2.5$ GeV/c for FTOF panel P2B. The vertical axis in the left-hand panel is the number of events from the Monte Carlo, *gemc* calculation divided by the bin size and the number of thrown events. The histogram in the right-hand panel is the number of events divided by the number of thrown events.

5 Simulation of FTOF Scintillator Response to Neutrons

The *gemc* code was run for neutrons striking one of the strips in each panel perpendicular to the plane of the panel at neutron momenta $p_n = 3.1$ GeV/c and $p_n = 8.0$ GeV/c. These momenta are at the upper and lower limits of the QE neutrons we expect to observe in panel P1A For each panel all of the other CLAS12 components between the target and the TOF panel were removed so those components would not alter the properties of the electrons striking the panel. The *gemc* command is much the same as the one above in Section 4 except for the choice of particle and momentum in the `BEAM_P` option of *gemc* which in the input file (`p1a.gcard` in Appendix A) is changed to the following.

```
<option name="BEAM_P" value="neutron,8.0*GeV, 25*deg, 0*deg" />
```

See Appendix A for more details about the input file. The options used in the command are described in Table 1 of Appendix A. The energy deposited for neutrons in the scintillator is shown in Figs. 9-12. The left-hand panel of Fig. 9 shows the distribution of deposited energy E_{dep} for all neutral particles (black histogram largely obscured by the red one) from primary neutrons with $p_n = 8.0$ GeV/c incident on panel P1A and perpendicular to the face of the panel. The distribution is broad; stretching out to an energy $E \approx 500$ MeV where E is the energy (known in simulation) of the particle as it enters the volume (the P1A scintillator panel here). The distribution is dominated by neutrons (70%) with the remainder composed mostly of photons produced by neutron reactions in the scintillator. The other important

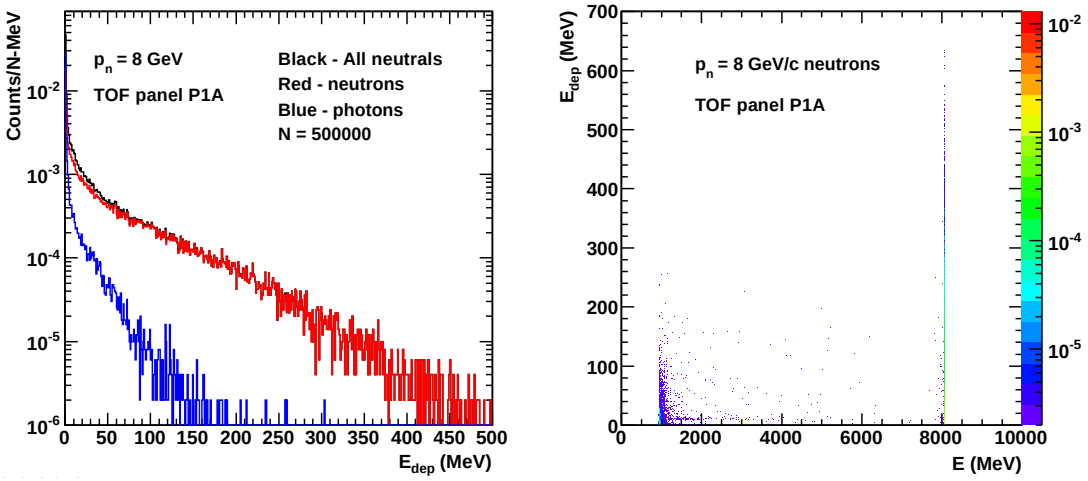

Figure 9: Energy deposited and particle energy in the FTOF scintillators for neutrons of momentum $p_n = 8.0$ GeV/c for FTOF panel P1A. The vertical axis in the left-hand panel is the number of events from the Monte Carlo, *gemc* calculation divided by the bin size and the number of thrown events. The histogram in the right-hand panel is the number of events divided by the number of thrown events and the bin size.

feature is the scale is much smaller than the comparable momentum for electrons (see, for example, Fig 4) reflecting the much lower detection efficiency of the scintillators for neutrons than electrons. The right-hand panel of Fig. 9 shows the distribution of E_{dep} versus E. The narrow ridge at $E = 8.0$ GeV is produced by the primary neutrons and there is a smaller group near $E = 1$ GeV from secondary neutrons produced by reactions in the scintillator.

Similar distributions are shown in Fig. 10 for a lower incident, primary neutron momentum $p_n = 3.1$ GeV/c. The deposited energy distribution for neutrons in the left-hand panel is softer; it does not extend to as high an energy as the higher-momentum neutrons in Fig. 10. On the other hand, the photon spectrum, which is produced by reactions in the material of the scintillator, is about the same in Figs. 9 and 10. The $E_{dep} - E$ spectrum in the right-hand panel of Fig. 10 has much the same features as the higher-momentum one in Fig. 9 except the ridge from the primary neutron is shifted to lower E.

The results for panels P1B and P2B (see Fig. 3) are shown in Figures 11-12. The deposited energy has the same features seen above. (1) The neutron spectrum is harder for higher-momentum incident neutrons and (2) the photon distribution changes little with incident neutron momentum.

6 Simulation of Neutron Detection Efficiency for Quasielastic $e - n$ Events

We now study the simulation of the quasielastic scattering of electrons from neutrons to extract the neutron scattering efficiency (NDE); an essential component of the G_M^n mea-

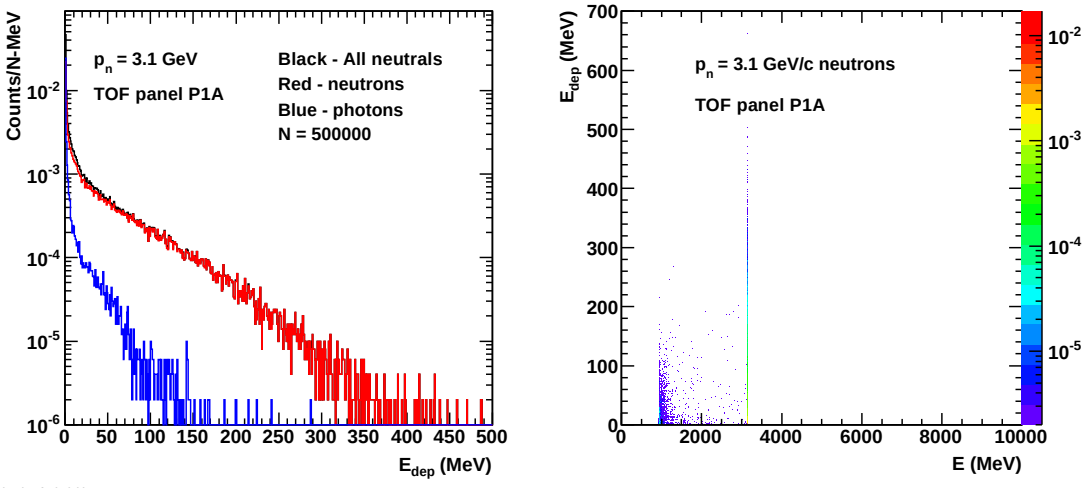

Figure 10: Energy deposited and particle energy in the FTOF scintillators for neutrons of momentum $p_n = 3.1$ GeV/c for FTOF panel P1A. The vertical axis in the left-hand panel is the number of events from the Monte Carlo, *gemc* calculation divided by the bin size and the number of thrown events. The histogram in the right-hand panel is the number of events divided by the number of thrown events and the bin size.

surement described above. This study will provide a baseline to understand the NDE in preparation for experiment E12-07-104. Quasielastic $e - n$ events were simulated assuming (1) a stationary neutron target and (2) an isotropic angular distribution. The first assumption provides a starting point for a future study of the NDE with a more realistic simulation of the Fermi motion of the neutron in deuterium. The second one enables us to obtain an adequate number of Monte Carlo events at large angles in a shorter period of time. These events were stored in a file in LUND format and then used as input to *gemc* [2] using the `INPUT_GEN_FILE` option (See Appendix A). The *gemc* command used here is listed in Appendix A.

Electrons were reconstructed with the code *Socrat* described in Ref. [3]. Reconstruction parameters can be found in Appendices B-C. A cut on the ratio $\Delta p_e/p_e^{angle}$ was required where

$$\Delta p_e = \frac{p_e^{meas} - p_e^{angle}}{p_e^{meas}} \tag{2}$$

and p_e^{meas} is the magnitude of the electron 3-momentum from the reconstruction (*Socrat*) and p_e^{angle} is the electron 3-momentum calculated using the electron polar angle θ_e taken from the reconstruction (*Socrat*) and assuming elastic scattering from the neutron. Fig. 13 shows the distribution of $\Delta p_e/p_e^{angle}$. This ratio was calculated event-by-event and required to be within ± 0.05 of zero. The expected resolution of CLAS12 of 1% [26]. The width of the central peak in Fig. 13 is a combination of the resolution of the magnitude of the momentum and the electron polar angle θ_e and has a width of about 1.3%. A second cut on E_{dep} was also required. The minimum value for the deposited energy in CLAS6 ($E_{dep} > 0.5$ MeV) was estimated from Ref. [27] and applied to all FTOF signals in *gemc*.

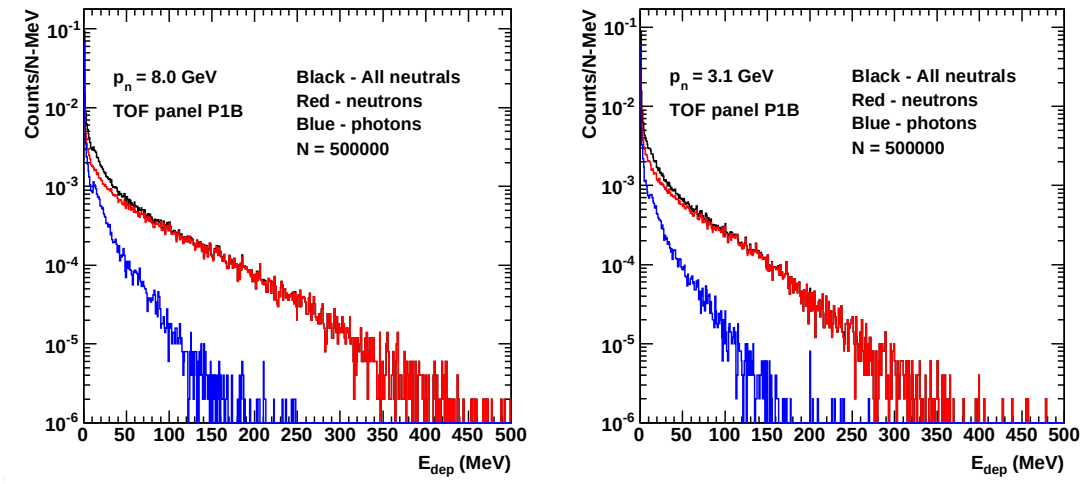

Figure 11: Energy deposited and particle energy in the FTOF scintillators for neutrons of momentum p_n = 8.0 GeV/c (left-hand panel) and p_n = 3.1 GeV/c (right-hand panel) for FTOF panel P1B. The vertical axis on each plot is the number of events from the Monte Carlo, *gemc* calculation divided by the bin size and the number of thrown events.

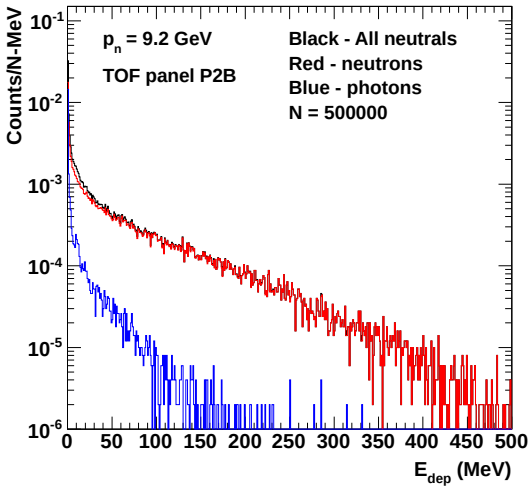

Figure 12: Energy deposited and particle energy in the FTOF scintillators for neutrons of momentum p_n = 9.1 GeV/c for FTOF panel P2B. The vertical axis on each plot is the number of events from the Monte Carlo, *gemc* calculation divided by the bin size and the number of thrown events.

Quasielastic neutrons were reconstructed in the following way. (1) Using only the reconstructed electron information and assuming elastic scattering off the neutron, the direction and momentum of the scattered neutron was calculated. Note here that our results for the neutron efficiency do not depend on the electron efficiency or acceptance since we start with

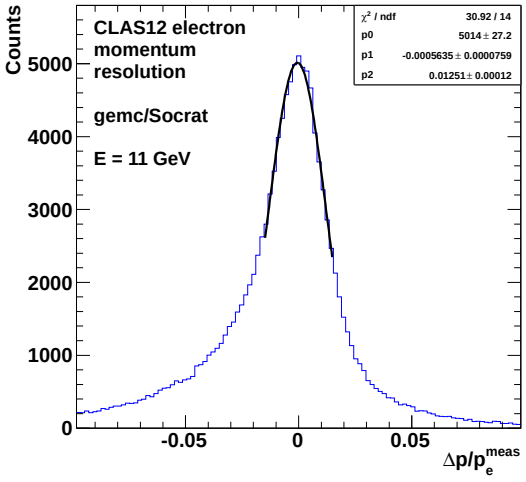

Figure 13: Distribution of $\Delta p_e/p_e^{meas}$ using the momentum from the Socrat reconstruction with the momentum calculated from the reconstructed electron angle and assuming quasielastic scattering.

a detected electron. (2) A neutron track was generated assuming the electron vertex as the starting point and using the calculated neutron 3-momentum to determine the direction from that vertex. (3) The intersection point of the neutron track and the plane of each FTOF panel in the expected CLAS12 sector was calculated. This task was done using the three points at the corners of the active area of the FTOF P1A and P1B panels to define a triangular plane, calculating the intersection point of this plane and the line of the neutron track, and using a theorem from analytical geometry to determine if the intersection point lay inside this triangle [28]. If the intersection point lay within the FTOF panel active area, this neutron was classified as 'found'. If the intersection point lay outside the active area, the event was rejected. We emphasize here that the struck panel was determined solely from the calculated direction of the neutron extracted from the measured electron information. In Figure 14 we show a schematic drawing to illustrate the algorithm. The panel (P1A or P1B) is the blue triangle and the predicted position of the quasielastic neutron is shown by the green cross on the face of the FTOF panel.

For the P2B panel the approach was modified because the scintillator panel is shaped like a trapezoid and not a triangle. The trapezoidal shape of the panel was used to form the bottom portion of a new triangle shown in Fig. 15. The outline of the P2B panel is shown by the yellow trapezoid and the triangle A (outlined in blue) is constructed so its base and two equivalent angles coincide with the bottom side and angles of the P2B trapezoid. The intersection of the neutron track with this new triangle was calculated and tested to see if it lay inside triangle A. If that condition was true, then the intersection point was required to lie close enough to the base of the isosceles triangle to be within the active area of the P2B panel shown in yellow in Fig. 15. if this second requirement for panel P2B was satisfied, the neutron was classified as 'found'. (4) The FTOF data was then scanned to see if one of the hits in the FTOF matched the expected position of the 'found' neutron. A

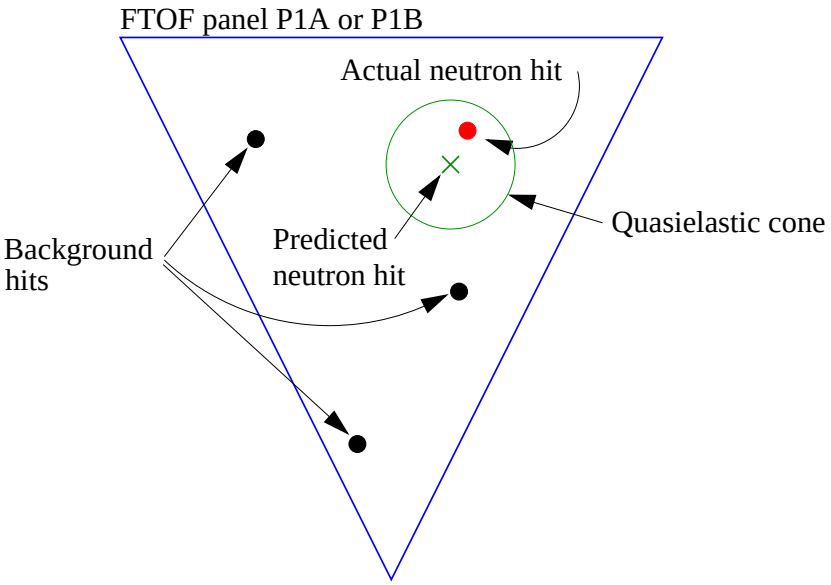

Figure 14: Schematic drawing showing the components of the algorithm used to select quasielastic neutrons in the FTOF panels in CLAS12. Drawing is not to scale.

ray was drawn from the vertex of the electron track to the position of a hit on the face of the FTOF panel and the angle γ was calculated between this ray and the one representing the direction of the 3-momentum of the found neutron. If this angle was less than 10°, the neutron reconstruction was deemed a success. If the angle was greater than 10°, the event was rejected. This 'quasielastic cone' is represented by the green circle in Figure 14. The reconstructed neutron hit is shown in red and lies within the cone while the other background hits are outside the cone. If more than one FTOF hit lay within this angular cone around the found neutron 3-momentum, then the hit with the smallest angle γ was selected. This algorithm was applied to all FTOF panels.

Fig. 16 shows the opening angle γ between the direction of the found neutron 3-

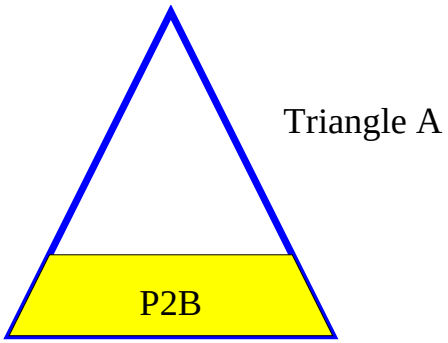

Figure 15: Schematic drawing of the geometry used to determine if an elastic neutron struck the active area of the P2B panel in the FTOF in CLAS12.

momentum and the ray going from the electron track vertex to each FTOF hit in panel P1B. The black histogram shows γ for all found neutrons that have an associated hit in any

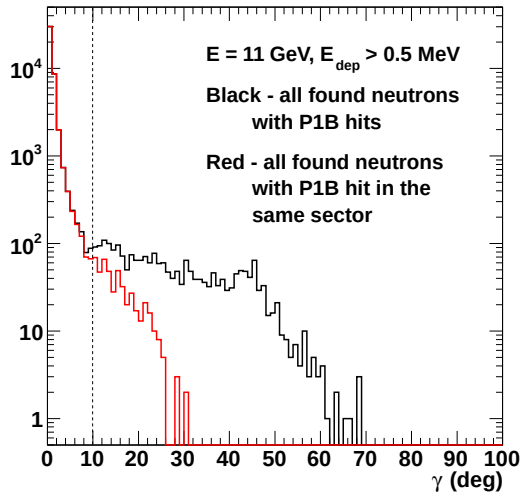

Figure 16: Opening angle between found neutron and TOF hit in panel P1B which lies in front of panel P1A. The vertical line shows position of cut to select neutrons.

FTOF panel. There is a rapid, exponential drop from the peak at $\gamma = 0°$ out to 10°. Beyond that range, the distribution of found neutrons with a P1B hit in the event is nearly flat and then drops rapidly again beyond 40° to zero. The red histogram shows the same distribution for all found neutrons with a FTOF hit that lay in the same sector as the found neutron. It closely follows the black histogram for all FTOF hits out to $\gamma = 10°$ and then diverges; continuing to fall rapidly to zero. The dashed line in Fig. 16 marks the position of the cut on γ used to select reconstructed neutrons. This value for the γ cut ($\gamma = 10°$) was originally used in the CLAS6 G_M^n analysis and it can be seen here that the cut excludes the region where background hits in other sectors start to become significant. About 99% of the events in the red histogram fall within the 10° cut.

The neutron detection efficiency (NDE) can now be extracted from the simulation. It is the ratio of reconstructed neutrons to found neutrons. Fig. 17 shows the momentum distribution of found (black) and reconstructed (red) neutrons in the left-hand panel. The found neutron spectrum is for neutrons that are expected to strike the active area of CLAS12 and may or may not have a coincident hit in the FTOF. The momentum distribution of found neutrons is peaked at high momentum. This abundance of high-momentum neutrons can be explained since it is associated with low-momentum, large-angle electrons in quasielastic scattering. These large-angle electrons are scattered into a region where CLAS12 has larger acceptance because it is away from the region at forward angles where the cryostat for the torus coils is merging and reducing the acceptance. The red histogram for the reconstructed neutrons has much the same shape, but reduced in size by about a factor of ten. The right-hand panel in Fig. 17 shows the NDE extracted from the distributions shown in the

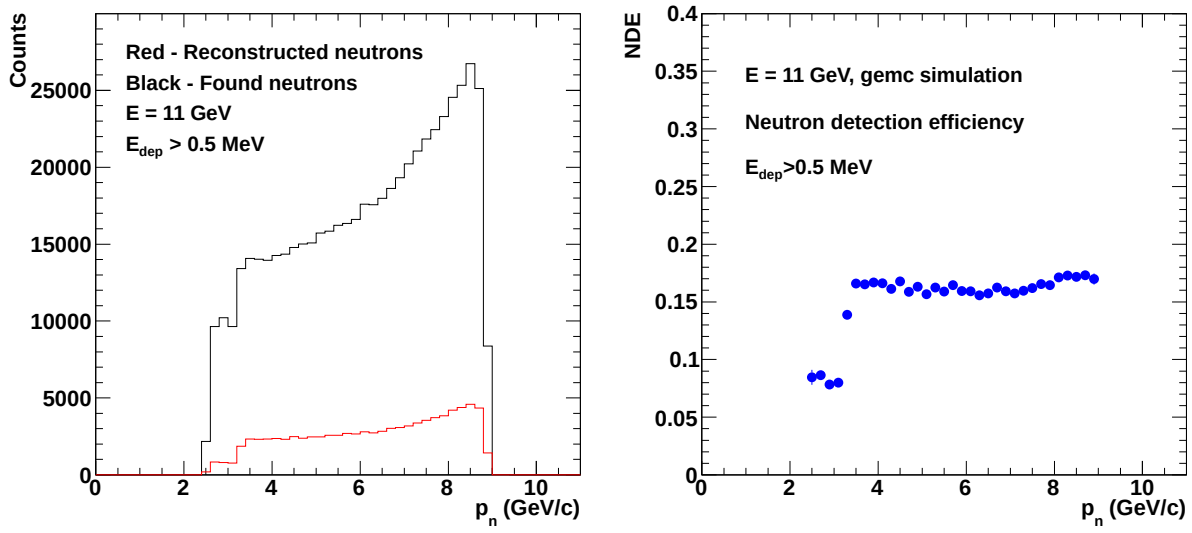

Figure 17: Histograms of found (black) and reconstructed (red) neutrons detected in FTOF are shown in the left-hand panel. The neutron detection efficiency derived from these results is shown in the right-hand panel.

left-hand panel. The simulated NDE (blue points) is largely flat over most of the momentum range and drops off rapidly at the limits of the acceptance. The drop in the efficiency at $p_n \approx 3$ GeV/c is due to edge of the P1B panel. Quasielastic neutrons at higher momentum and more forward angles have to pass through both P1B and P1A panels. At larger neutron angle (and lower momentum for QE neutrons), the particles only encounter the P2B panel which has lower efficiency than the combined P1A+P1B panels.

The response of the neutron detection efficiency to changes in the E_{dep} threshold was studied. As mentioned above the value used here was the CLAS6 value taken from Ref. [27]. The results of changing this minimum value for E_{dep} are shown in Fig. 18. The average NDE for the P1A+P2B panels is $15.6 \pm 0.2\%$ at the nominal CLAS6 threshold and rises to a maximum of $17.6 \pm 0.2\%$ when the threshold is reduced to zero. Turning the threshold up has only a modest effect on the neutron detection efficiency.

The detection efficiency for quasielastic neutrons was measured in the E5 run period and presents an opportunity to challenge our simulations here with data. During the E5 run the $^1\mathrm{H}(e, e'\pi^+)n$ reaction provided a source of tagged or 'found' neutrons where the neutron momentum was known from the electron and pion kinematics. The found neutrons were then matched with hits in the CLAS6 time-of-flight system. The P1A and P2B panels to be used in CLAS12 *gemc* were originally part of the CLAS6 time-of-flight system. We take this opportunity to compare the measured efficiency of the P1A and P2B panels with the *gemc* simulation of the same FTOF panels.

To compare the *gemc* simulation and the E5 NDE measurement we focus only on the P1A and P2B panels. The P1B panel in front of P1A was turned off in the simulation. The results are shown in Fig. 19. The left-hand panel shows the momentum spectra for

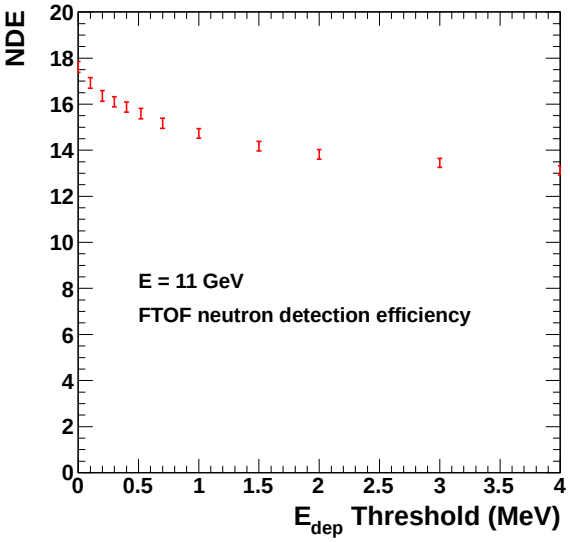

Figure 18: Dependence of the neutron detection efficiency (NDE) for quasielastic neutrons as a function of the minimum deposited energy E_{dep} is shown.

found and reconstructed neutrons. The shapes are qualitatively similar to the ones in the left-hand panel of Fig. 17. The right-hand panel in Fig. 19 shows the NDE extracted from the momentum spectra (blue points). The dip in the efficiency at $p_n \approx 3$ GeV/c is caused by QE neutrons that strike a gap between panels P1A and P2B. This gap is covered by the P1B panel in the full CLAS12 detector. For $p_n > 4$ GeV/c the neutrons were detected in panel P1A and have a roughly constant efficiency of about 8%. At the lowest neutron momenta below the dip in the CLAS12 simulation, the efficiency returns to 8% where the neutrons are striking panel P2B. The E5 measurement of the NDE is shown as the black points in Fig. 19. The E5 measured NDE rises rapidly from zero and reaches a plateau at $p_n \approx 2$ GeV/c and at an efficiency of 8%. There is good agreement within the experimental uncertainty between the measured E5 NDE and the one simulated with *gemc*. It bears emphasizing that the simulated and measured results agree even though two different reactions are used (elastic scattering for *gemc* and the $^1\mathrm{H}(e, e'\pi^+)n$ reaction for E5).

We now summarize the work described in this CLAS-NOTE. We have simulated the production and reconstruction of quasi-elastically scattered electrons and neutrons in CLAS12 with *gemc* [2] and *Socrat* [3]. We have studied the properties of the deposited energy and efficiency of the CLAS12 FTOF system to establish a baseline for the future. We have simulated the extraction of the neutron detection efficiency using QE neutrons and found an efficiency of 16% for panels P1A and P1B combined together and a value of 8% for panel P2B. A comparison of the simulated efficiency using only panels P1A and P2B (that are being reused from CLAS6) with the measured values from the E5 run (using the $^1\mathrm{H}(e, e'\pi^+)n$ reaction) shows good agreement. For future work to prepare for the CLAS12 G_M^n measurement we will add the effects of Fermi motion to the target neutron and develop a simulation of the $^1\mathrm{H}(e, e'\pi^+)n$ reaction that will be used to extract the neutron detection efficiency in

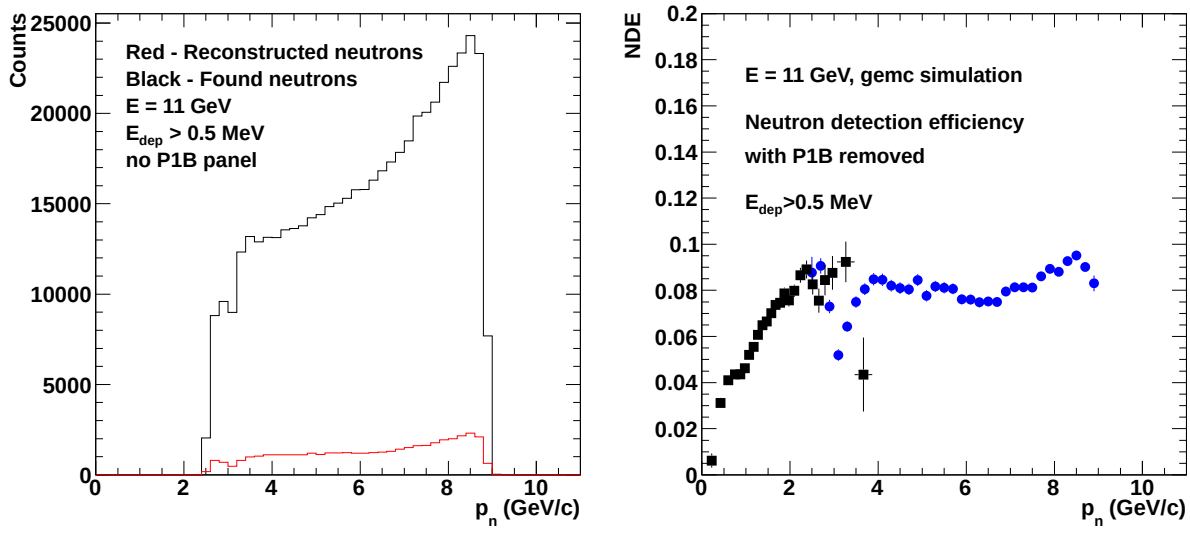

Figure 19: Histograms of found (back) and reconstructed (red) neutrons detected in FTOF panels P1A and P2B only are shown in the left-hand panel. The neutron detection efficiency derived from these results is shown in the right-hand panel (blue points) along with the NDE measured at $E = 4.2$ GeV in CLAS6 during the E5 running period (black points). The dip in the efficiency is due to a small gap between the P1A and P2B panels.

the CLAS12 G_M^n experiment (E12-07-104).

This work is supported by US Department of Energy grant DE-FG02-96ER40980 and Jefferson Science Associates. We acknowledge Elton Smith for helpful comments on this CLAS-NOTE.

References

[1] G.P. Gilfoyle et al. Experiment E12-07-104, Jefferson Lab, Newport News, VA, 2007.

[2] M. Ungaro. *gemc* - geant4 montecarlo. Technical report, Jefferson Lab, 2011.

[3] S. Procureur. Socrat: a software for clas12 reconstruction and tracking. CLAS-Note 2008-015, Jefferson Lab, 2008.

[4] Nuclear Science Advisory Committee. *The Frontiers of Nuclear Science*. US Department of Energy, 2007.

[5] J. Lachniet, A. Afanasev, H. Arenhövel, W. K. Brooks, G. P. Gilfoyle, D. Higinbotham, S. Jeschonnek, B. Quinn, M. F. Vineyard, et al. Precise Measurement of the Neutron Magnetic Form Factor G_M^n in the Few-GeV^2 Region. *Phys. Rev. Lett.*, 102(19):192001, 2009.

[6] W. Bartel et al. *Nucl. Phys. B*, 58:429, 1973.

[7] G. Kubon et al. *Phys. Lett. B*, 524:26–32, 2002.

[8] A. Lung et al. *Phys. Rev. Lett.*, 70(6):718–721, Feb 1993.

[9] H. Anklin et al. *Phys. Lett. B*, 428:248–253, 1998.

[10] B. Anderson et al. *Phys. Rev. C*, 75:034003, 2007.

[11] R. G. Arnold et al. Measurements of transverse quasielastic electron scattering from the deuteron at high momentum transfers. *Phys. Rev. Lett.*, 61(7):806–809, Aug 1988.

[12] S. Rock et al. Measurement of Elastic Electron-Neutron Cross Sections up to $Q^2 = 10$ $(GeV/c)^2$. *Phys. Rev. Lett.*, 49(16):1139–1142, Oct 1982.

[13] W. M. Alberico, S. M. Bilenky, C. Giunti, and K. M. Graczyk. Electromagnetic form factors of the nucleon: New fit and analysis of uncertainties. *Phys. Rev. C (Nuclear Physics)*, 79(6):065204, 2009.

[14] G.A. Miller. *Phys. Rev. C*, 66:032201, 2002.

[15] M. Guidal, M.V. Polyyakov, A.V. Radyushkin, and M. Vanderhaeghen. *Phys. Rev. D*, 72:054013, 2005.

[16] I. C. Cloet, G. Eichmann, B. El-Bennich, T. Klahn, and C. D. Roberts. Survey of nucleon electromagnetic form factors. *Few Body Syst.*, 46:1–36, 2009.

[17] C.E. Hyde-Wright and K.deJager. Electromagnetic Form Factors of the Nucleon and Compton Scattering. *Ann. Rev. Nucl. Part. Sci.*, 54.

[18] H. Anklin et al. *Phys. Lett. B*, 336:313–318, 1994.

[19] G. Kubon et al. *Phys. Lett. B*, 524:26–32, 2002.

[20] E. E. W. Bruins et al. Measurement of the neutron magnetic form factor. *Phys. Rev. Lett.*, 75(1):21–24, Jul 1995.

[21] G.P. Gilfoyle, W.K. Brooks, S. Stepanyan, M.F. Vineyard, S.E. Kuhn, J.D. Lachniet, L.B. Weinstein, K. Hafidi, J. Arrington, D. Geesaman, R. Holt, D. Potterveld, P.E. Reimer, P. Solvignon, M. Holtrop, M. Garcon, S. Jeschonnek, and P. Kroll. Measurement of the Neutron Magnetic Form Factor at High Q^2 Using the Ratio Method on Deuterium. E12-07-104, Jefferson Lab, Newport News, VA, 2007.

[22] J.D. Lachniet, W.K. Brooks, G.P. Gilfoyle, B. Quinn, and M.F. Vineyard. A high precision measurement of the neutron magnetic form factor using the CLAS detector. CLAS Analysis Note 2008-103, Jefferson Lab, 2008.

[23] J. Allison et al. Geant4 developments and applications. *IEEE Transactions on Nuclear Science*, 53:270–278, 2006.

[24] Wikipedia. Qt (framework) — wikipedia, the free encyclopedia, 2011. [Online; accessed 27-June-2011].

[25] The CLAS12 TDR Editorial Board. The CLAS12 Technical Design Report. Technical report, Thomas Jefferson National Accelerator Facility, Newport News, VA, 2008.

[26] The Hall B 12 GeV Upgrade CDR Editorial Board. The Hall B 12 GeV Upgrade Preconceptual Design Report. Technical report, Thomas Jefferson National Accelerator Facility, Newport News, VA, 2005.

[27] K. Loukachine. *Measurement of the Polarization of the phi(1020) in Electroproduction*. PhD thesis, Virginia Polytechnic Institute, 2000.

[28] Wikipedia. Line-plane intersection — wikipedia, the free encyclopedia, 2011. [Online; accessed 26-July-2011].

A *gemc* Input

The command used to run *gemc* from the command line in batch mode to study the response of the P1A panel alone is below. Options are stored in the file `p1a.gcard` which is also displayed below along with Table 1 describing this set of options.

```
gemc  -gcard=p1a.gcard
```

Input file `p1a.gcard`:

```
<gcard version= "1.0" date= "2011-9-09" author= "G.Gilfoyle">

<!-- Forward Detectors: -->
   <sqltable name="SECTOR"/>
   <sqltable name="OTOF"/>

<!-- Beamline -->
   <sqltable name="moeller_shield"/>

<!-- Detectors Existance -->
   <detector name="OTOF_Panel_1b">
      <existence exist="no" />
   </detector>

<!-- Options -->

<option name="USE_QT" value="0" />
<option name="BEAM_P" value="e-, 9.25*GeV, 25*deg, 0*deg" />
<option name="SPREAD_P" value="0.0*GeV, 0*deg, 0*deg"  />
<option name="OUTPUT" value="evio, results.ev" />
<option name="N" value="10" />
<option name="PRINT_EVENT" value="3" />
<option name="HALL_MATERIAL" value="Vacuum" />
<option name="USE_PHYSICSL" value="gemc" />
<option name="LUMI_EVENT" value="0,0*ns,2*ns" />
<option name="NO_FIELD" value="all" />

</gcard>
```

The command used to run *gemc* from the command line in batch mode to study quasielastic neutron production in CLAS12 is below. Neutron and electron 4-vectors were produced by another program and stored in a file in LUND format. This file was used as input to *gemc*. Options are stored in the file `nde.gcard` which is reproduced below. Table 1 has descriptions of the options.

```
gemc  -gcard=nde.gcard
```

Option	Description	Option	Description
USE_QT	Turn graphics on/off.	OUTPUT	Event file output.
N	Number of events	PRINT_EVENT	Print intermediate event results.
BEAM_P	Choose particle type and 3-momentum.	USE_PHYSICSL	Choose parameter set for materials.
gcard	File to select geometry components.	HALL_MATERIAL	Turn on/off effects of air in hall.
SPREAD_P	Width of particle 3-momentum ranges.	LUMI_EVENT	Parameters for beam luminosity test.
NO_FIELD	Turn CLAS12 magnetic field on/off.	ENERGY_CUT	Turns off tracking below this value.
SCALE_FIELD	Increase/decrease the magnetic field.	INPUT_GEN_FILE	Input event file.
HALL_FIELD	Turn on magnets.	SAVE_ALL_MOTHERS	Save additional information.

Table 1: Table of options used in *gemc* input file `p1a.gcard`.

Input file `nde.gcard`:

```
<gcard version= "1.0"  date= "2011-9-09" author= "G.Gilfoyle">

<!-- Central Detectors: -->
   <sqltable name="FST"/>

<!-- Forward Detectors: -->
   <sqltable name="SECTOR"/>
   <sqltable name="OTOF"/>
   <sqltable name="DC12"/>

<!-- Beamline -->
   <sqltable name="moeller_shield"/>

<!-- Magnets: -->
   <sqltable name="torus"/>

<!-- Detectors Existance -->
   <detector name="OTOF_Panel_1b">
      <existence exist="yes" />
   </detector>

<!-- Options -->

<option name="USE_QT" value="0" />
<option name="INPUT_GEN_FILE" value="nInput1.dat" />
```

```
<option name="OUTPUT" value="evio, nde_results.ev" />
<option name="N" value="1000" />
<option name="PRINT_EVENT" value="200" />
<option name="HALL_MATERIAL" value="Vacuum" />
<option name="USE_PHYSICSL" value="gemc" />
<option name="SCALE_FIELD" value="1" />
<option name="SAVE_ALL_MOTHERS" value="1" />
<option name="HALL_FIELD" value="srr-solenoid" />
<option name="ENERGY_CUT" value="100*MeV" />
<option name="LUMI_EVENT" value="0,0*ns,2*ns" />
```

B Socrat Parameter Input

```
// This is the option file to run the Socrat tracking code
// Author: S.Procureur, May 2008, v1.0

//the electron beam energy in GeV, only important for Neutron Tracking
Ebeam   11.0

// run the neutron tracking code (1) or not (0)
Neutron Tracking    1
// run the forward tracking code (1) or not (0)
Forward Tracking 1
// run the central tracking code (1) or not (0)
Central Tracking 0

// vertex fit on (1) or off (0) (both central and forward track must be on!)
Vertex Fit 0

// Events from Geant (1) of from internal Socrat routine (0)
Geant 1

// if Geant mode, specify the path to the Geant output
//GFile gemc.root
//GFile /home/moog/ec/clas12EC3.root
//GFile results.root
GFile mmass.root

// Mode: batch (1) or interactive (0)
Mode 1

// Number of events to process (batch mode only, without Geant)
Events 100000

// Save a DC or BST display of last event (interactive mode only)
DispEvent DC 1
DispEvent BST 1

// Do the final fit or not (using Kalman Filter)
Kalman Filter 1

// Fill the output root tree (1) or not (0)
Outtree 1

// Debug mode (more variables in output tree) on (1) or off (0)
Debug 0

// Verbosity, how much do you want printed to the screen while socrat runs?
Verbosity 0
```

```
// Cut on deposited energy in DC and FST (in MeV)
DC Edep 0.0001
SVT Edep 0.02
CTOF Edep 1.0

// Use linear interpolation for torus field estimation (should be 1!)
Linear Interp 1

// orientation of first wire in DC: +6 (1) or -6 (-1)
DC Firstangle 1

// ministagger in the DC (in microns)
DC Ministag    500.

// torus polarity (1: electrons go back to the beam; -1: opposite)
Torus Polarity 1

// Use the Forward Tracker (1) or not (0)
FST use 0

// fraction of dead channels in the FST (in %)
FST dead    0.0

//-------------------------------------------------------------------
// if Geant mode is not used, you need to specify the phase space for
// the internal track generator type of charged particle (numbering
// scheme from PDG, eg proton is 2212, electron is 11)
Central Particle 11
Forward Particle 11
// range in p (GeV/c)
Central Prange 0.25 1.5
Forward Prange 5 8

// range in theta (polar angle, in degrees)
Central Thetarange 35 125
Forward Thetarange 15 40

// range in phi (azimuthal angle, in degrees)
Central Phirange 50 60
Forward Phirange 50 60

// z length of the target (in m, vertex will be generated randomly inside it)
Target length 0.00

// occupancy in each of the DC regions (in %)
```

```
DC occ 0 0 0
// background rate in FST, if used (in MHz/ layer)
FST rate 0
// background rate in BST, if used (in MHz/ layer)
BST rate 0
// Multiple scattering on (1) or off(0)
Mult Scat 1
// Print the hits information
Print Hit 0

// introduce some misalignments (in mm and mrad!)
Misalign BST Z 0 0 0 0
Misalign BST R 0 0 0 0
Misalign BST Phi 0 0 0 0
Misalign DC R 0 0 0
Misalign DC Tilt 0 0 0
Misalign DC Angle1st 0 0 0
Misalign FST Z 0 0 0
Misalign FST Phi 0 0 0
Misalign Solenoid 0 0 0
Misalign Torus 0 0 0

// Internal param (change speed, don't change if you don't know it!)
Time Accel 4.0e-13 5
```

C Socrat Tracking Parameters

```
// This is the parameter file to run the Socrat tracking code
// Author: S.Procureur, June 17th, 2008, v1.1

FI2 iteration 30
KF iteration 2
DC Dwire 0.18 5.0
FST InterMargin 0.02
FST Dphi 0.02
FST DRadius 0.004 -0.002
DC LRiter 8
BST InterMargin 0.1
BST VertexDist 0.008
BST Prange 0.1 4.0
CTOF TimeWindow 60 80
BST Dphi 0.4 0.25 0.7 0.7 0.4
BST distP4 0.07 0.01
BST cosP234 0.75
//Torus FieldInt 1.20 1.17 1.00 0.9
Torus FieldIntp -3.20 0.0695 -0.000667 0.000000531 0.0000000182 -2.85 -0.0230 0.00316
Torus FieldIntm -4.30 0.131 -0.00212 0.0000165 -0.0000000472 -2.89 -0.0317 -0.0192
FT CovMat1 0.03 0.08 0.5
FT CovMat2 0.03 0.08 0.5
FT CovMatN 0.03 0.08 0.2
DCFST Rmatching 0.01
FST MultResol 1. 100000.
CT CovMat zphi 0.002 0.0005 1.0 0.25
CT CovMat mom 0.04 0.01 0.1 0.05
BST MultResol 3.0
VERTEX DistRZ 0.01 0.01
```